processes

MDPI

Article

The Influence of Coal Body Structure on Coal Fines' Output Characteristics in the Southern Qinshui Basin

Junshan Ren [1,2,3], Zhou Zhang [1,2,3,*], Liru Xing [1], Pengxiang Wang [1], Wanying Yu [1] and Piao Long [1]

[1] School of Resources and Environment, Henan Polytechnic University, Jiaozuo 454000, China; rjs19980120@163.com (J.R.); xlr082725@163.com (L.X.); a18236856202@163.com (P.W.); 15655533298@163.com (W.Y.); lopo228@163.com (P.L.)
[2] Henan International Joint Laboratory for Unconventional Energy Geology and Development, Henan Polytechnic University, Jiaozuo 454000, China
[3] Collaborative Innovation Center of Coalbed Methane and Shale Gas for Central Plains Economic Region, Jiaozuo 454000, China
* Correspondence: zhangzhou@hpu.edu.cn

Abstract: Large amounts of coal fines are discharged from coalbed methane wellheads in the Qinshui Basin, obstructing the continuity of drainage; their extraction poses significant hazards. This paper recognized the coal body structure of 30 coalbed methane wells in the study region, using the integrated identification method of logging curve and tectonic curvature. The research found that the primary structural coal output of coal fines concentration averaged 0.237 g/L, the average content of particle size 10–100 μm was 58.88%, the average range of particle size 1–10 μm was 22.91%, and the main form was irregular columns and lumps. The average concentration of fractured structural coal fines was 1.169 g/L, the average content of particle size 10–100 μm was 41.73%, the average range of particle size 1–10 μm was 31.77%, and the main form was balls and lumps. The average concentration of granulated-mylonitic structured coal fines was 3.156 g/L, the average content of particle size 10–100 μm was 25.26%, the average range of particle size 1–10 μm was 57.59%, and the coal fines were mainly in the form of clusters and flaky aggregates.

Keywords: coalbed methane; Qinshui Basin; coal fines' output characteristics; coal body structure; control mechanism

Citation: Ren, J.; Zhang, Z.; Xing, L.; Wang, P.; Yu, W.; Long, P. The Influence of Coal Body Structure on Coal Fines' Output Characteristics in the Southern Qinshui Basin. *Processes* **2024**, *12*, 656. https://doi.org/10.3390/pr12040656

Academic Editor: Carlos Sierra Fernández

Received: 18 February 2024
Revised: 16 March 2024
Accepted: 19 March 2024
Published: 26 March 2024

1. Introduction

China's coalbed methane resources are rich, with triple benefits of energy, safety, and environmental protection [1–3]. The coalbed methane production process commonly exists in coal fines' output problems. On the one hand, coal fines migrate to clog the natural fracture system of coal seams or the pore-fracture of proppant-filled layers, reducing reservoir permeability and affecting gas transport through pore fractures [4–7]; on the other hand, coal fine particles clog the well bottom sieve tubing and the pump suction inlet, resulting in a poor closure of the vane, leakage of the pump, reduction in the efficacy of the discharge pumps, easily causing the jamming of the pumps, and the need for frequent pump inspections, which damages the continuity of gas production in CBM wells, affecting the gas production potential [8,9].

Some scholars have already developed a lot of research on coal fines. Pranesh [10] investigated the relationship between coal fines yield and clay minerals—kaolinite was investigated by core oil drive experiments—and revealed that it is easier to produce coal fines with a more significant proportion of clay content during CBM drainage depressurization, because of the decrease in reservoir pressure and the increase in effective stress, which leads to the shear damage of the coal skeleton. The coal rock gradually loses its original stress balance and the elastic self-adjustment of the coal rock leads to the production of coal fines [11,12]. In the drilling process, the drilling tool grinds with the coal seam and

produces coal fines due to mechanical damage. This part of the coal fines is generally coarser and the concentration and amount of coal fines produced in horizontal wells are higher than those produced in straight wells [13,14]. In hydraulic fracturing, the coal rock is crushed by stress to produce coal fines [15,16]. The current understanding is that coal fines are mainly influenced by a mixture of geological and engineering aspects [17,18]. Among them, the coal body structure has an important influence on the generation of coal fines. The most direct way to identify the coal body structure is to drill a core shaft [19]. However, the coal body structure is easily damaged during coring and it is difficult to directly identify many coal body structures using core data, due to the number of coring wells and the cost. Logging data are abundant, continuous, and relatively low-cost, and logging data for coal body structure identification has been widely used. Zhuang's [20] prediction of coal fines' output concentration in CBM wells was established using a correlation model between GSI value and coal fines' volume fraction. Zhang [21] identified and classified the coal body structure of Yangquan block by analyzing the deformation and distribution of coal seams in underground wells and combining their response characteristics on logging curves on this basis. Xiao [22] determined the coal body structure using the logging curve and the modeling of the random classification of the coal body structure. Wei [23] predicted the coal body structure in the Liulin mine by constructing a component analysis-support vector machine coal body structure prediction model.

Previous research results mainly focus on the identification of coal bodies and the influencing factors of coal fines output, but have not yet systematically elucidated the controlling effects of coal fines' output pattern on different coal body structures. In this paper, the coal body structures of 30 coalbed methane wells were identified using the integrated identification method of logging curve and tectonic curvature analysis. At the same time, we use a vacuum filtration device, laser particle size meter, and field emission scanning electron microscope to study the coal fines' output characteristics in the Panhe and Shizhuang South Block. The aim of this study is to reveal the output characteristics of coal fines under different coal body structures and to discuss their control mechanisms, so as to provide a basis for adjusting the reasonable discharge mining system.

2. Geological Setting

The Qinshui Basin is located in the southeastern region of Shanxi Province, China. It is a basin developed on the basement of the Paleozoic, between the Taihang and Huoshan uplift zones, and faults are not well developed in the basin (Figure 1) [24]. The Panhe block and the Shizhuang South block are located on the southeastern slope of the Qinshui Basin.

The tectonic development of the Panhe block is simple, with NNE anticline and syncline aligned, and faults are not developed in the area. The stratigraphy is gentle and the central part of the block develops a broad and gentle short-axis syncline, favorable for the enrichment of CBM. The sedimentary sequence of the basin is sequentially Carboniferous, Permian, and Quaternary. Taiyuan Group No.15's central coal seam has a moderate burial depth and thickness ranging from 0.80 to 6.17 m. The structure of the coal seam is relatively simple, containing a small amount of gangue, generally 1~2 layers [25]. No.15's coal seam has an average reservoir pressure gradient of 0.81 kPa/m, a moderate gas content of 20 m^3/t, a permeability ranging from 0.08 to 1.45 mD, and a 25.8 kPa/m stress gradient. Shizhuang South Block is a single-slope tectonic structure, in general, and the area is affected by many phases of tectonic movement, forming alternately superimposed anticline and syncline and tectonic circles, with more developed faults in the north and mainly compound folds in the south. The basement of the basin is composed of metamorphic rocks from the Upper Archean to Lower Proterozoic [26]. The sedimentary filling sequence within the area includes the Paleozoic Ordovician, Carboniferous, Permian, Mesozoic Triassic, and Cenozoic Quaternary coal seam of Shanxi Group. The No.3 seam is the main coal seam now being mined and its thickness is 3~11 m, with an average of 6.39 m, it has 1~2 layers of gangue with a thickness of about 0.3 m in the middle and the gas content of the coal seam is generally 4.1~23.3 m^3/t [27,28].

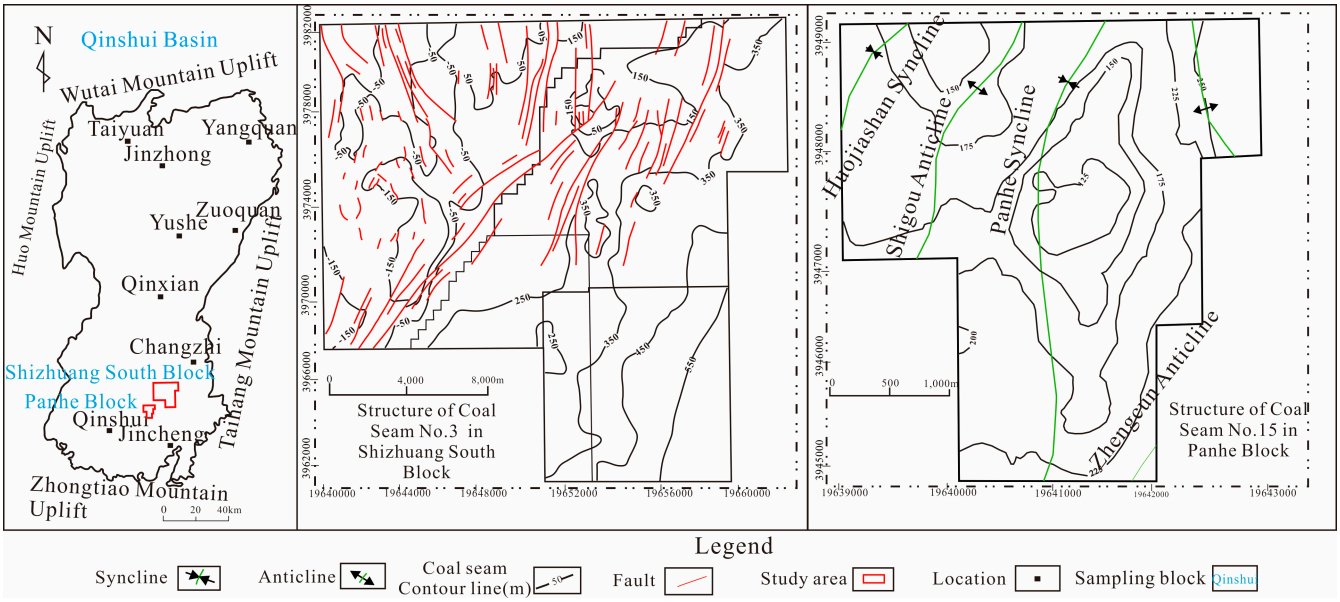

Figure 1. Outline map of the geology of the study area.

3. Experiments and Methods

3.1. Sample Collection

Selecting 30 coalbed methane wells from the Panhe and Shizhuang South blocks in the Qinshui Basin to collect 59 samples, we used a plastic bottle with a capacity of 500 mL to pick up the oil pipe drainage outlet, where considerable coal fines outputs occurred during the production process (Figure 2). Samples from water outlets of CBM wells were collected in three batches, immediately encapsulated to prevent oxidation and contamination, and were transported to the laboratory for analysis.

Figure 2. Coal fines' solution samples.

Investigation of the basic parameters of coal fines were carried out concerning the national standard (Table 1). The moisture content of coal fines is 2.22~3.42%, the volatile matter is 25.94~34%, and the ash content is 53.83~69.93%. The ash content of coal rock samples taken from roadway workings was 14.74~28.33%, with an average of 15.16%. Coal fines have a much higher ash content than coal rocks, as the ash is mainly the product of burning inorganic minerals, indicating that the coal fines have a high mineral content.

Table 1. Basic parameters for proximate analysis of samples.

Sample Type	Sample Number	M_{ad}	V_{ad}	A_{ad}
Coal fines	PH-117H1	2.32	30.77	65.23
	PH-117H2	2.46	29.89	65.77
	PH74-10X1	3.42	26.33	69.93
	PH-119H4	2.69	25.94	53.83
	PH-116H1	3	34	58.87
	PH-111H2	2.22	26.83	65.55
Coal rock	ZS1	2.6	6.3	14.76
	ZS2	2.65	6.34	14.74
	PH63	6.17	8.08	15.99
	PH8-2	1.7	7.37	28.33

3.2. Experimental Program Design

3.2.1. Concentration

The mass concentration of coal fines was tested using the weighing method in the laboratory, using a 500 mL sand-core filtration unit with a vacuum pump (Figure 3). First, the filter membrane was dried in a drying oven at 55 °C for two hours and cooled to room temperature for weighing. After shaking the water sample of coal fines evenly, 100 mL was taken and poured into a measuring cup. After filtration, the filter membrane with coal fines was dried in the oven under the same conditions for 12 h. After weighing, the membrane was continued to be dried until the weight no longer changed [29].

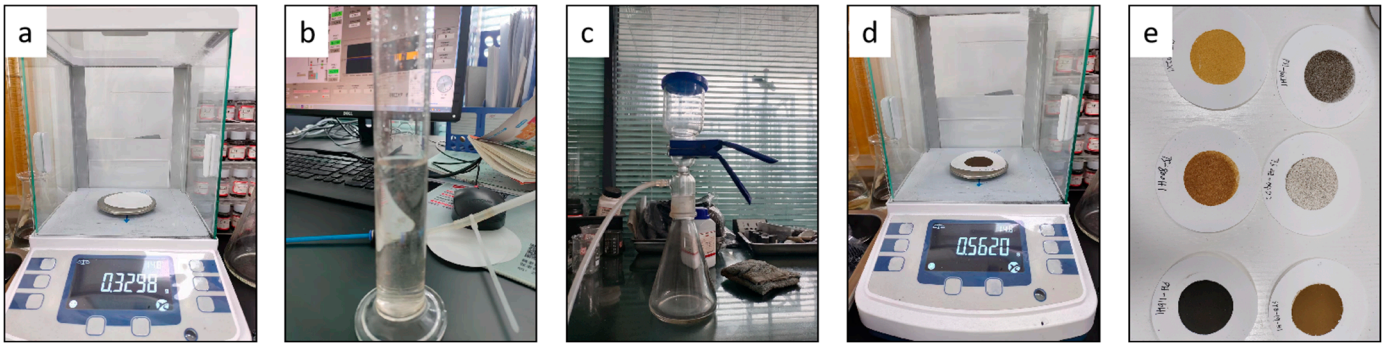

Figure 3. Coal fines' concentration test steps. (**a**) Weigh the filter paper. (**b**) Transfer the coal fines solution to a measuring cylinder. (**c**) Filtration. (**d**) Weigh the coal fines and filter paper after filtration. (**e**) Dried coal fines.

3.2.2. Particle Size

We used an ultra-high-speed intelligent particle size analyzer (Mastersize 3000, Malvern, UK) to test and analyze the particle size of coal samples. The test range was from 0.015 to 3500 μm and the test was carried out using the wet method, using distilled water as the dispersant and selecting the supernatant of the coal fines solution for testing.

3.2.3. Morphological

Coal fines' water samples were filter dried. The morphology of the coal fines particles was observed under high magnification using a scanning electron microscope (Zeiss Sigma 300, Oberkochen, Germany) and the morphology of coal fines from different samples was analyzed and compared. Coal fines particles are usually considered electrically non-conductive and must be sprayed in advance with gold.

4. Results and Discussion

4.1. Coal Body Structure Identification

4.1.1. Logging Curves

There is no uniform standard for the division of coal body structures at either a domestic or international level. With the increase in coal body fragmentation, the pore cleavage in the coal rock increases, leading to a relative decrease in its density, increased electrical conductivity, and decreased resistivity value. Natural gamma is also susceptible to the influence of coal seam ash and formation water, resulting in large fluctuations in amplitude. Raw potential logging shows the apparent anomalies at the permeable layers, and the negative peaks of the curves are generally sandstones with permeability. Well wall collapse often occurs during drilling, resulting in different degrees of dilatancy, and changes in well diameter can reflect the structural characteristics of the coal body of the well wall, based on the exploration well data, the well logging interpretation of the CBM production wells from which the coal fines samples were taken. The classification of coal body structures with logging data is mainly based on the physical differences between coal body structures, and different geological conditions in different regions lead to differences in logging response [30]. This paper mainly categorizes the coal body structure into primary structural, fractured structural, granulated-mylonitic structural, and cretaceous coal, using the logging curve [31]. The logging curve data of Panhe No.15 coal and Shizhuang South No.3 coal were counted to determine the range of logging response parameters of different coal body structure types (Table 2), and the main parameters used were bulk density (DEN), deep lateral resistivity (RD), natural gamma (GR), natural potential (SP), and well diameter expansion rate (CAL).

Table 2. Logging response coal body structure classification criteria.

Block	Type of Coal Body Structure	Parameter Characteristics				
		DEN (g/cm^3)	RD (Ω·m)	GR (API)	SP (mv)	CAL (%)
Panhe No.15 coal seam	Primary structure	1.5~1.6	>3000	<100	<−20	<10
	Fractured structure	1.45~1.55	>1000	<100	<0	10~30
	Granulated-mylonitic structure	<1.5	<1000	<80	>0	>30
Shizhuang South No.3 coal seam	Primary structure	1.3~1.6	>5000	<60	<0	<10
	Fractured structure	1.3~1.5	>2000	<60	<0	10~30
	Granulated-mylonitic structure	<1.4	<2000	<40	<50	>30

4.1.2. Tectonic Curvature

The coal seam is in a tectonic stress field and will bend due to tectonic stress; the degree of such bending can be described by tectonic curvature. Tectonic curvature is a mathematical quantitative description of the geometrical form of the geological structure, which reflects the strength of deformation under stress. It can be used in coal and CBM geology to recognize the anxiety and the deformation of coal seams and to determine their structure [32]. Applying the grid difference method to calculate the tectonic curvature can better reflect the size of the primary curvature of the local tectonic morphology and then reflect the development of some regional small tectonics. Large curvature indicates strong deformation. Mathematically, the tectonic curvature can be calculated using the following formula:

$$K = \frac{|z''|}{(1 + z'^2)^{\frac{3}{2}}} \quad (1)$$

There are infinitely many curvature curves over a point on the plane, but only one curvature value maximizes, called the tremendous significant curvature K_{max}. A square

grid was used to dissect the coal seam floor (Figure 4) and the difference equation is shown below:

$$z' = \frac{f(x_{i+1}, y_j) - f(x_{i-1}, y_j)}{2\Delta h} \quad (2)$$

$$z'' = \frac{f(x_{i+1}, y_j) + f(x_{i-1}, y_j) - 2f(x_i, y_j)}{\Delta h^2} \quad (3)$$

In the formula, $z = f(x,y)$—elevation of the base plate of a coal seam; K—curvature at a point on the floor of a coal seam; (i,j)—differential grid coordinates; and Δh—differential grid point spacing.

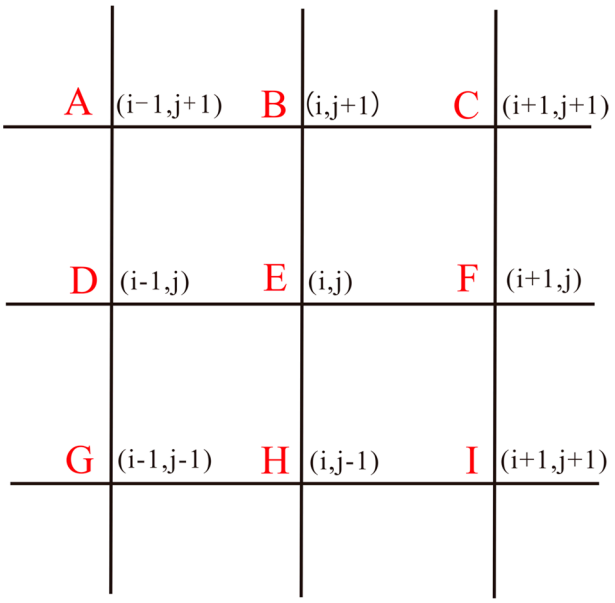

Figure 4. Differential grid schematic.

The results of (2) and (3) are brought into Equation (1) to calculate the curvature value. For the DF direction, the curvature value in one order at point E can be calculated. Similarly, the tectonic curvature in the remaining directions can be calculated. Since the coal seam is subjected to the maximum tensile or compressive stress at the maximum curvature value, the maximum curvature at point E is taken as the final curvature value, according to Equation (4).

$$K_E = \max(K_{DF}, K_{BH}, K_{AI}, K_{CG}) \quad (4)$$

Based on the integrated identification method of logging curves and tectonic curvature, the coal body tectonics of 30 CBM production wells in the study area were identified. Coal body tectonic types with total thickness greater than 50% were selected to represent the coal body tectonic types of the wells, and different coal body tectonic types in the plane were developed to different degrees in the same coal seam. Based on the results of tectonic curvature calculation, tectonic curvature contour maps were drawn, as shown in Figure 5. The degree of deformation of the target coal seam was classified into different zones, as shown in Table 3. The high deformation zones in Panhe block are distributed throughout the whole area, while the high deformation zones in the Shizhuang South block are mainly distributed near the faults in the north and west.

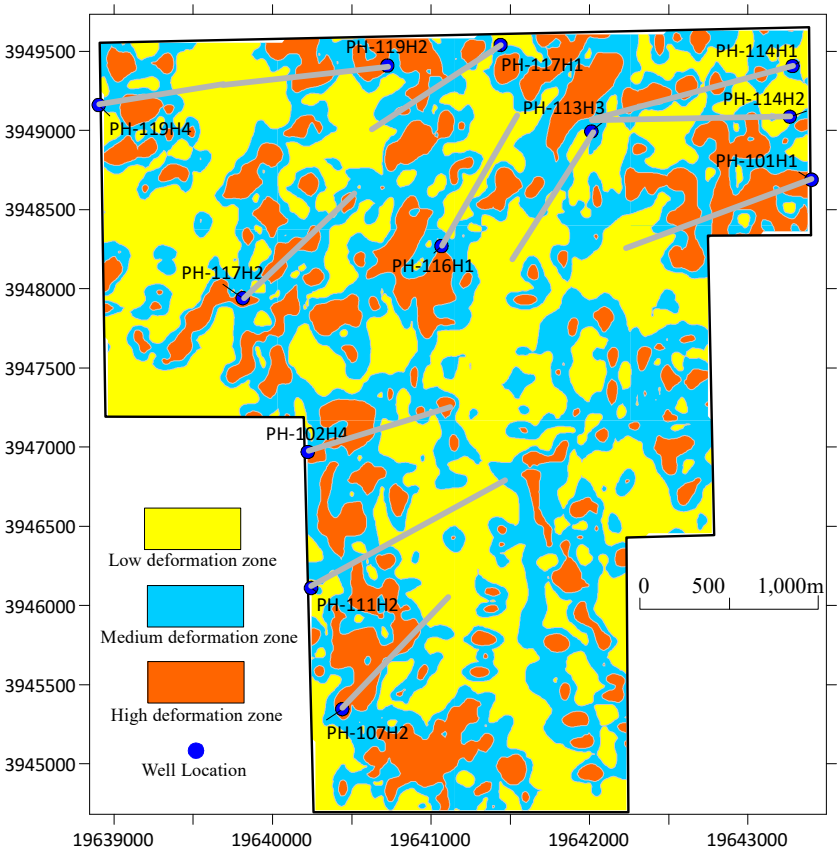

(**a**) Panhe Block

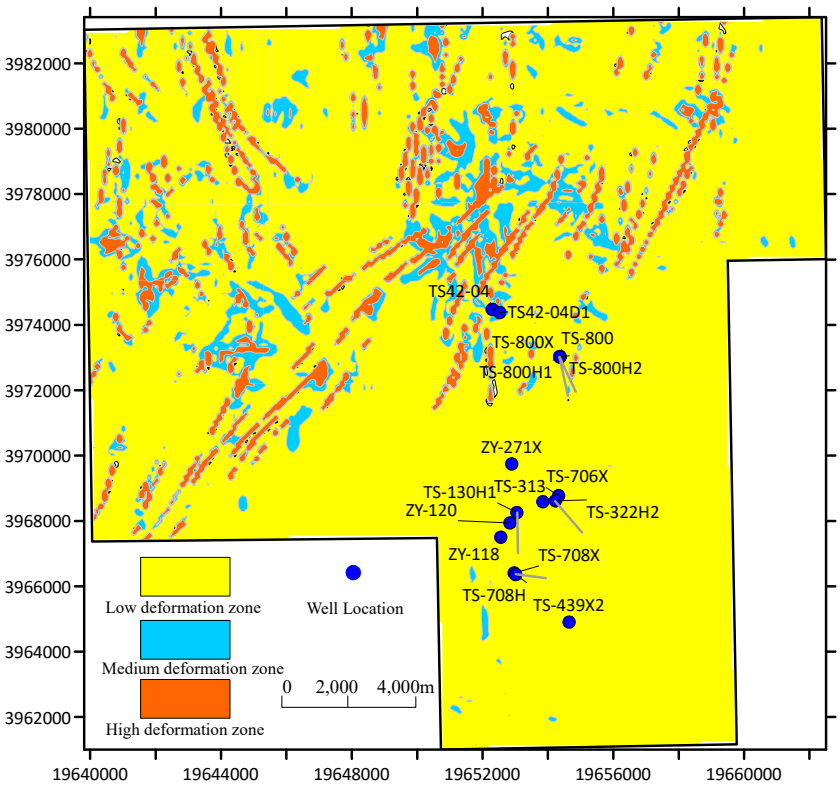

(**b**) Shizhuang South block

Figure 5. Tectonic curvature deformation zoning.

Table 3. Coal deformation degree partitioning based on tectonic curvature.

Curvature Classification	Absolute Value of Tectonic Curvature/10^{-4} m^{-1}
High deformation zone	>10
Medium deformation zone	5~10
Low deformation zone	<5

The coal body structures were identified using both the logging response method and structural curvature method; the results of identification are shown in Table 4. The matching degree of coal body structure recognition is found to be high. Granulated-mylonitic coals dominate the coal fines samples extracted from the Panhe block, and the samples from the Shizhuang South block are dominated by primary-fractured structural coals.

Table 4. The coal body structure recognition results.

Sample Number	Logging Identification	Absolute Value of Tectonic Curvature/10^{-4} m^{-1}	Tectonic Curvature Recognition	Adoption of Results
PH-101H1	primary structure	1.78–15.73	primary-mylonitic structure	primary-mylonitic structure
PH-101X1	primary structure	1.64	primary structure	primary structure
PH-102H4	fractured structure	9.09–13.71	fractured-granulated structure	fractured-granulated structure
PH-107H2	fractured structure	1.68–19.83	primary-mylonitic structure	fractured-granulated structure
PH-111H2	primary structure	3.22–6.33	primary-fractured structure	primary-fractured structure
PH-113H3	fractured structure	2.79–6.65	primary-fractured structure	fractured structure
PH-114H1	granulated-mylonitic structure	7.04–9.46	fractured structure	fractured-mylonitic structure
PH-114H2	fractured structure	2.88–9.08	primary-fractured structure	fractured structure
PH-116H1	granulated-mylonitic structure	3.95–10.43	primary-granulated structure	granulated structure
PH-117H1	granulated structure	3.52–4.35	primary structure	primary-granulated structure
PH-117H2	granulated-mylonitic structure	9.18–14.88	fractured-mylonitic structure	granulated-mylonitic structure
PH-119H2	fractured structure	0.53–10.13	primary-granulated structure	fractured-granulated structure
PH-119H4	primary-fractured structure	0.54–7.12	primary-fractured structure	primary-fractured structure
PH74–10X1	primary structure	7.87	fractured structure	primary-fractured structure
TS-130H1	primary structure	0.80–1.37	primary structure	primary structure
TS-313	granulated-mylonitic structure	0.46	primary-fractured structure	primary-fractured structure
TS-322H2	primary structure	0.83-1.23	primary structure	primary structure
TS42-04	primary structure	5.94	fractured structure	primary-fractured structure

Table 4. *Cont.*

Sample Number	Logging Identification	Absolute Value of Tectonic Curvature/10^{-4} m^{-1}	Tectonic Curvature Recognition	Adoption of Results
TS42-04D1	fractured structure	13.04	granulated-mylonitic structure	fractured-mylonitic structure
TS-439X2	fractured structure	0.26	primary structure	primary-fractured structure
TS-706x	primary structure	0.60	primary structure	primary structure
TS-708H	primary-fractured structure	1.29–1.75	primary structure	primary structure
TS-708X	primary-fractured structure	0.60	primary structure	primary structure
TS-800	primary structure	2.65–6.55	primary-fractured structure	primary structure
TS-800H1	primary-fractured structure	0.57–2.68	primary structure	primary-fractured structure
TS-800H2	primary-fractured structure	2.39	primary structure	primary structure
TS-800X	fractured structure	2.66	primary structure	primary-fractured structure
ZY-118	primary structure	0.51–5.23	primary-fractured structure	primary structure
ZY-120	primary structure	0.74	primary structure	primary structure
ZY-271X	fractured structure	1.09	primary structure	primary-fractured structure

4.2. Control of Coal Body Structure on Coal Fines' Concentration

Statistical analysis of the three sampling results of 30 CBM wells (Table 5) showed that the output coal fines' concentration of CBM wells ranged from 0.02 to 22.0 g/L, with an average of 1.609 g/L. Following the identification results of the coal body structure (Table 4), the coal structure with the most significant degree of fragmentation was selected as a criterion to classify the coal structure of the sampled wells into three categories. Among them, the output coal fines' mass concentration of CBM wells dominated by primary structural coal is 0.02~1.574 g/L, with an average of 0.237 g/L. The coal fines' mass concentration of CBM wells dominated by fractured structural coal is 0.053~7.195 g/L, with an average of 1.169 g/L. The output coal fines' mass concentration of CBM wells dominated by granulated-mylonitic structural coal is 0.156~22.0 g/L, with an average of 3.156 g/L (Figure 6). As the coal structure becomes more and more broken, the output concentration of coal fines gradually increases.

Table 5. The coalbed methane well coal fines concentration statistics.

Sample Number	Mass Concentration of Coal Fines (g/L)			
	First Test	Second Test	Third Test	Average Value
PH-101H1	1.700	0.297	0.792	0.930
PH-101X1	0.698	0.281		0.489
PH-102H4	0.400		0.156	0.278
PH-107H2	0.933	0.406	1.312	0.884
PH-111H2	7.195	4.398		5.797
PH-113H3	0.200	0.315	0.061	0.192
PH-114H1	7.143	0.831	1.864	3.279
PH-114H2	0.300	0.162	0.210	0.224

Table 5. *Cont.*

Sample Number	Mass Concentration of Coal Fines (g/L)			
	First Test	Second Test	Third Test	Average Value
PH-116H1	2.258		3.315	2.786
PH-117H1	20.000	0.513	1.854	7.456
PH-117H2	22.000	0.717		11.359
PH-119H2	0.900	0.323	1.338	0.854
PH-119H4	0.169	0.124	4.008	1.434
PH74-10X1	2.800		0.288	1.544
TS-130H1	0.227			0.227
TS-313	0.050			0.050
TS-322H2	0.200			0.200
TS42-04	0.290			0.290
TS42-04D1			0.371	0.371
TS-439X2	0.172	0.053		0.113
TS-706x	0.071			0.071
TS-708H	0.167	0.076		0.121
TS-708X	0.020	1.574		0.797
TS-800	0.150	0.033		0.092
TS-800H1	0.377		0.039	0.208
TS-800H2	0.357	0.035	0.032	0.141
TS-800X	0.100			0.100
ZY-118			0.074	0.074
ZY-120	0.025			0.025
ZY-271X	0.200			0.200

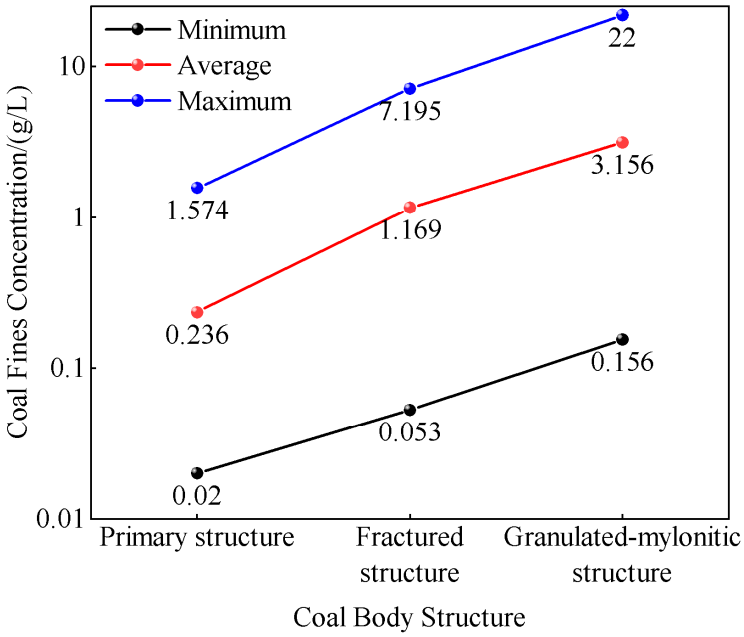

Figure 6. Average concentration values for different coal body structures.

4.3. The Role of the Coal Body Structure in the Control of Coal Fines' Particle Size

The experimental results for the particle size of coal fines are as follows (Table 6): Primary structural coals with particle sizes between 10 and 100 μm accounted for 18.27% to 97.63%, with an average content of 58.88%, and those with particle sizes between 1 and 10 μm accounted for 1.65% to 58.41%, with moderate content of 22.91%; fractured structural coals with particle sizes between 10 and 100 m accounted for 7.71% to 66.87%, with an average range of 41.73%, and those with particle sizes between 1 and 10 μm accounted for 14.77~77.92%, with moderate content of 31.77%; the particle size of the granulated-

mylonitic structural coal accounted for 10.65~49.25% in 10–100 μm sized particles, with an average content of 25.26%, and the percentage of the particle size of 1–10 μm ranged from 41.14% to 81.5%. With the broken structure of the coal body, the proportion of coal fines with a particle size of 10–100 m gradually decreases, the proportion of particles sized between 1 and 10 m gradually rises, and the overall particle size tends to become smaller, with a small amount of large particles larger than 1000 m or no coal fines.

Table 6. Particle size data for coal fines.

Main Coal Body Structure	Sample Number	D10	D50	D90	Coal Fines Content of Different Particle Sizes/%				
					<1 μm	1–10 μm	10–100 μm	100–1000 μm	>1000 μm
Primary structure	PH-101X1	10.889	34.543	77.844	1.72	7.39	86.74	4.15	0
	TS-130H1	2.78	17.7	1380	3.06	25.77	49.04	6.02	16.11
	TS-708H	19.731	39.012	71.521	0	1.65	97.63	0.72	0
	TS-708X	2.543	15.264	56.051	5.22	31.77	61.31	1.7	0
	TS-800H1	2.87	25.6	1520	3.66	18.67	50.4	8.31	18.96
	TS-800H2	4.02	30.6	1680	2.2	16.68	48.79	8.94	23.39
	ZY-118	0.58	2.9	15.884	23.32	58.41	18.27	0	0
Fractured structure	PH-111H2	0.784	2.74	8.69	14.37	77.92	7.71	0	0
	PH-113H3	3.039	14.937	36.687	3.71	27.95	66.87	1.47	0
	PH-114H2	3.93	28.9	120	1.66	20.95	63.3	13.51	0.58
	PH-119H4	4.23	23.4	1330	2.01	19.29	57.71	5.72	15.27
	PH74-10X1	1.42	5.61	584	5.23	61.34	13.29	14.78	5.36
	TS42-04	4.49	65.8	1790	1.99	14.77	42.92	14.9	25.42
	TS-439X2	1.67	20	1020	4.91	31.94	47.82	4.85	10.48
	ZY-271X	54.2	121	199	0	0	34.21	65.79	0
Granulated-mylonitic structure	PH-101H1	1.03	4.18	19.2	9.43	68.44	21.96	0.17	0
	PH-102H4	1.436	6.595	21.128	7.03	60.32	32.55	0.1	0
	PH-107H2	1.3	8.43	246	6.97	46.44	20.45	26.14	0
	PH-114H1	1.35	6.61	339	6.01	54.22	15.26	24.51	0
	PH-116H1	1.79	7.34	23.2	3.44	61.94	34.13	0.49	0
	PH-117H1	1.48	14.8	513	5.33	41.14	12.66	40.7	0.17
	PH-117H2	1.13	3.85	10.1	7.85	81.5	10.65	0	0
	PH-119H2	2.05	10.9	36	3.28	42.51	49.25	3.61	1.35
	TS42-04D1	1.46	6.96	16.705	7.79	61.76	30.45	0	0

4.4. Control Mechanism of Coal Body Structure on Coal Fines' Morphology

The morphology of coal fines produced by primary structural coal is dominated by irregular columnar and massive particles with distinctive angles and poor rounding, and the particle size is large, which can exceed 50 μm (shown in Figure 7a). The morphology produced by the fractured structure coal has a significant variation in particle size, less pronounced angularity, and is dominated by spherical shapes, containing some irregular lumps (shown in Figure 7b). The morphology of coal fines' output from the granulated-mylonitic structural coal varies in size, mainly rare cluster and flake aggregates, interspersed with a few columnar and wedge-shaped particles, and the edges of the crushed particles are mostly sub-circular, a little arcuate, with good rounding, while a large number of fine particles attached to the particle surface can be observed (shown in Figure 7c).

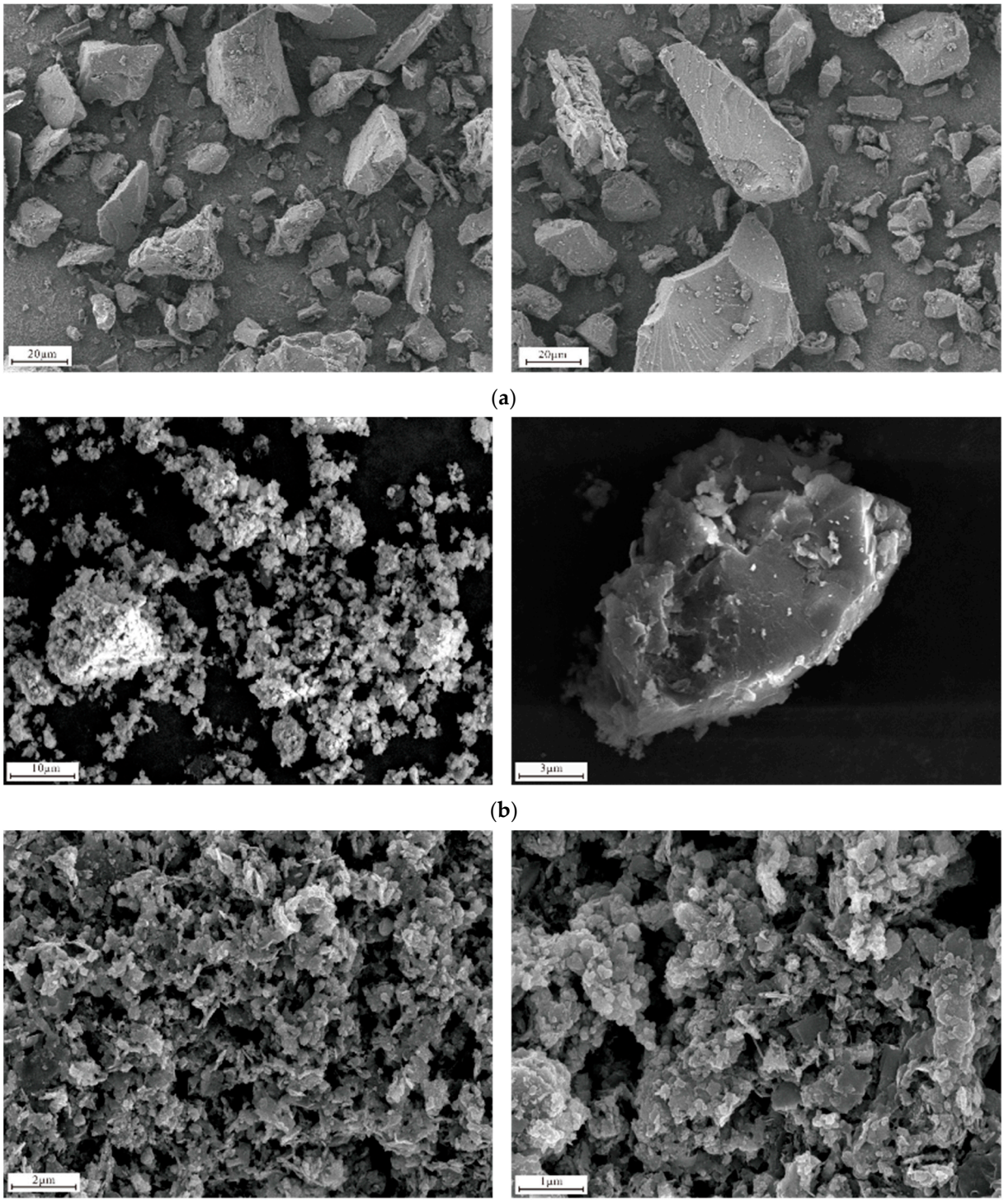

Figure 7. Characteristics of coal fines' output morphology. (**a**) Primary structural coal output coal fines morphology. (**b**) Fractured structural coal output coal fines morphology. (**c**) Granulated-mylonitic structural coal output coal fines morphology.

4.5. Control Mechanism of the Output Characteristics of Coal Fines

Coal seams have strong non-homogeneity, and there are considerable differences between the physical properties of different types of coal body structural coal reservoirs [33]. Primary structural coals and fractured structural coals are relatively structurally intact, due to the low degree of destruction, and produce low amounts of coal fines. In the tectonic

coal region of development, due to substantial tectonic stress, the coal seams are softer, the clay mineral aggregates, especially, have poor adhesion to the skeletal particles, while the bonding between crystals is weak. They are easily detached from the surface of the coal matrix, thus increasing the concentration. Meanwhile, when the hydrodynamic conditions of the coal seam are changed, part of the coal fines deposited in the fracture channel is stimulated and transported out of the fracture channel into the discharge pipeline, resulting in a high coal fines concentration in the pipeline.

The size range of coal fines decreases as the coal seam breaks up. Primary structural coal is less affected by the later tectonic action and has a more complete preservation of the coal body structure; the design produces coal fines with larger particle size under fluid erosion and stress. The coal seam developed via fractured structural coal is subjected to the later tectonic action, the coal body structure is damaged to a certain extent, and the produced particle sizes are different; the coal seam dominated by granulated-mylonitic structural coal is most seriously injured under the tectonic solid stress in the later stage, and it produces many coal fines. Under the tectonic stable pressure of the last phase, the coal body structure is most severely damaged, the coal seam is softer and produces many coal fines, the mylonitic coal is easily dispersed upon contact with water, and it is easier to be decomposed by friction during the later handling process. Therefore, in the coal seam crushed-grained mylonitic coal output, coal fines are generally small and have a more limited particle size distribution scale.

The microscopic morphological observation of coal fines shows that the coal fines' morphology is related to the structure of the coal body, and it is hypothesized that the reason for the difference in the morphology of it's particles is mainly related to the degree of coal deformation. Primary-fractured structural coal has a low degree of destruction and a relatively complete structure, primarily deformed by fracture under the shear action of stress, and the morphology of the output coal fines is mainly characterized by irregular lumps and columns, which are usually angular. The granulated-mylonitic structure coal is most affected by the late tectonic stress; the coal seam is softer and the cracks contain more primary coal fines, which undergo high-intensity fluid shear and inter-particle friction, resulting in the gradual rounding of the particles, and the morphology tends to be sub-angular or sub-circular—the morphology characteristics of the output coal fines with the type of coal body structure.

4.6. The Significance of Coal Fines' Management

By studying the impact of coal body structure on coal fines' production, it is beneficial to improve the utilization efficiency of coalbed methane well capacity and reduce the waste caused by incompatible processes. Currently, coalbed methane well production basically requires hydraulic fracturing to create fractures. With the same geostress, areas with fractured coal structures have shorter extensions of fracture ends caused by fracturing, resulting in more coal fines production, which severely damages the coal reservoir and affects the continuity of subsequent coalbed methane well gas production. When choosing the fracturing layer, it is advisable to avoid areas with soft coal layers and opt for indirect fracturing of the coal seam roof rather than direct fracturing of the coal seam. In wells, coal fines are in a slurry form and traditional coal fines fishing operations are ineffective, necessitating coal fines flushing operations. Directional and horizontal wells with serious coal fines issues should use jet pumps to reduce pump blockage caused by settling, but this will lead to a large amount of water entering the coal seam, making it difficult for some wells to recover production.

Coal body structure is an important factor affecting coal fines production. Research has shown that the highest concentration of coal fines production occurs in granulated-mylonitic structure coal, with a smaller particle size, which severely affects the production and extraction of coalbed methane wells in structural coal development areas. Therefore, in the production process of coalbed methane, implementing underground monitoring of coal fines' concentration and conducting warning and intelligent processing are challenges

that need to be addressed during the extraction process. The proposed technical solution involves installing suitable concentration meters in short sections of tubing in the wellbore within structural coal development areas to monitor the coal fines' concentration in real-time. When the underground coal fines' concentration exceeds the set value, the surface analysis control system will analyze and process the situation, automatically shutting down the extraction pump operation and, subsequently, automatically opening the surface water injection pump to inject water into the well for coal fines' dilution. When the coal fines' concentration is detected to reach a safe extraction range, the underground extraction pump is started for normal production, reducing the impact of coal fines in the wellbore upon extraction.

5. Conclusions

The concentration, particle size, and morphology of coal fines produced by different coal body structures were studied by collecting coal fines solutions from wellheads of the Panhe Block and Shizhuang South Block. The research methods include coal body structure delineation by combining logging and tectonic curvature, the weighing process to measure the concentration, laser particle sizer to analyze the particle size, and field emission scanning electron microscopy to view the shape. The mechanism of coal body structure on coal fines output was elaborated.

(1) Primary structure dominated seams with an average coal fines' output concentration of 0.237 g/L. The average coal fines' mass concentration dominated by fractured-structure coals is 1.169 g/L. The output of coal fines from granulated-mylonitic structure coals is 3.156 g/L.
(2) The average content of primary structural coal particle size is 58.88% in 10–100 μm, and the average range of particle size 1–10 μm is 22.91%; the moderate content of fractured structural coal particle size is 41.73% in 10–100 μm, and the average range of particle size 1–10 μm is 31.77%; the moderate content of granulated-mylonitic structural coal particle size is 25.26% in 10–100 μm, and the average range of particle size 1–10 μm is 57.59%.
(3) The coal fines produced by different types of structural coal differ in morphology. Primary structural coal has mostly irregular columnar and massive coal fines, fractured structural coal has mostly spherical and huge coal fines, and granulated-mylonitic structural coal produces mostly clustered and flaky aggregates.
(4) Primary structural coal structures, as a whole, are intact, with low concentrations and large particle sizes, mainly irregular columnar and massive particles; fractured structural coal is damaged by tectonic stress, with increasing concentrations, decreasing particle sizes, and inconspicuous corners; and granulated-mylonitic structural coal is the most affected by the later tectonic stress, with large quantities of coal fines, generally small sizes, and the morphology usually exists in the form of aggregates.

Author Contributions: Conceptualization, J.R.; methodology, J.R. and Z.Z.; validation, J.R. and Z.Z.; writing—original draft preparation, J.R., Z.Z. and L.X.; writing—review and editing, J.R., P.W., W.Y. and P.L. All authors have read and agreed to the published version of the manuscript.

Funding: This research was funded by Key Projects of the National Natural Science Foundation of China (Grant Nos. 42230814) and Henan Province Science and Technology Research Project (Grant Nos. 222102320140).

Data Availability Statement: Some or all of the data during this study are available from the corresponding author upon request.

Conflicts of Interest: The authors declare that the research was conducted in the absence of any commercial or financial relationships that could be construed as potential conflicts of interest.

References

1. Zhou, F.; Hou, W.; Allinson, G.; Wu, J.; Wang, J.; Cinar, Y. A feasibility study of ECBM recovery and CO_2 storage for a producing CBM field in Southeast Qinshui Basin, China. *Int. J. Greenh. Gas Control* **2013**, *19*, 26–40. [CrossRef]
2. Xu, X.; Rui, X.; Fan, Y.; Yu, T.; Ju, Y. Forecasting of Coalbed Methane Daily Production Based on T-LSTM Neural Networks. *Symmetry* **2020**, *12*, 861. [CrossRef]
3. Qin, Y.; Shen, J.; Shi, R. Strategc value and choice on construction of large CMG industry in China. *J. China Coal Soc.* **2022**, *47*, 371–387.
4. Chen, Y.; Ma, Z.; Ma, D.; Zhang, Z.; Li, W.; Yang, F.; Ji, Y.; Peng, T. Characteristics of the Coal Fines Produced from Low-Rank Coal Reservoirs and Their Wettability and Settleability in the Binchang Area, South Ordos Basin, China. *Geofluids* **2021**, *2021*, 5560634. [CrossRef]
5. Tao, S.; Tang, D.; Xu, H.; Li, S. The influence of flow velocity on coal fines output and coal permeability in the Fukang Block, southern Junggar Basin, China. *Sci. Rep.* **2017**, *7*, 14124. [CrossRef]
6. Guo, Z.; Hao, V.P.N.; Hussain, F. A laboratory study of the effect of creep and fines migration on coal permeability during single-phase flow. *Int. J. Coal Geol.* **2018**, *200*, 61–76. [CrossRef]
7. Bai, T.; Chen, Z.; Aminossadati, S.M.; Rufford, T.E.; Li, L. Experimental investigation on the impact of coal fines generation and migration on coal permeability. *J. Pet. Sci. Eng.* **2017**, *159*, 257–266. [CrossRef]
8. Lan, W.; Wang, H.; Yang, S.; Zheng, C.; Liu, Y.; Chen, S. Study on the migration of pulverized coal in CBM wellbore. *J. Pet. Sci. Eng.* **2017**, *156*, 740–747. [CrossRef]
9. Wang, D.; Wang, Z.; Cai, X. Experimental study on coal fines migration and effects on conductivity of hydraulic fracture during entire coalbed methane production period. *Geoenergy Sci. Eng.* **2023**, *223*, 211555. [CrossRef]
10. Pranesh, V.; Balasubramanian, S.; Kumar, R.S.; Sakthivel, R.; Rajkumar, P.; Ravikumar, S. Kaolinite flakes and coal fines production in lignite core under ambient conditions: A case study of Neyveli Lignite Field at Cauvery Basin, Southern India. *J. Nat. Gas Sci. Eng.* **2019**, *64*, 72–80. [CrossRef]
11. Zou, Y.S.; Zhang, S.C.; Zhang, J. Experimental Method to Simulate Coal Fines Migration and Coal Fines Aggregation Prevention in the Hydraulic Fracture. *Transp. Porous Media* **2014**, *101*, 17–34. [CrossRef]
12. Han, W.; Li, Y.; Wang, Y.; Ni, X.; Wang, L.; Zhou, Y. Characterization of Coal Fines and their Production Controlling Factors: A Case Study from Southern Qinshui Basin, China. *Nat. Resour. Res.* **2023**, *32*, 1777–1794. [CrossRef]
13. Zhang, A.; Cao, D.; Wei, Y.; Rufford, T.E. Characterization of fines produced during drainage of coalbed methane reservoirs in the Linfen block, Ordos Basin. *Energy Explor. Exploit.* **2020**, *38*, 1664–1679. [CrossRef]
14. Han, W.; Wang, Y.; Li, Y.; Ni, X.; Wu, X.; Yang, J.; Zhao, S. Coal Fines Migration, Deposition, and Output Simulation during Drainage Stage in Coalbed Methane Production. *Energy Fuels* **2021**, *35*, 4901–4913. [CrossRef]
15. Zhang, X.; Hu, S.; Hao, Y.; Feng, G.; Li, S.; Chen, Z. Effect of Coal Fine Retention on the Permeability of Hydraulic Propped Fracture. *Rock Mech. Rock Eng.* **2022**, *55*, 6001–6014. [CrossRef]
16. Awan, F.U.R.; Keshavarz, A.; Akhondzadeh, H.; Al-Anssari, S.; Al-Yaseri, A.; Nosrati, A.; Ali, M.; Iglauer, S. Stable Dispersion of Coal Fines during Hydraulic Fracturing Flowback in Coal Seam Gas Reservoirs—An Experimental Study. *Energy Fuels* **2020**, *34*, 5566–5577. [CrossRef]
17. Wei, Y.; Li, C.; Cao, D.; Wang, A.; Zhang, A.; Yao, Z. The effects of particle size and inorganic mineral content on fines migration in fracturing proppant during coalbed methane production. *J. Pet. Sci. Eng.* **2019**, *182*, 106355. [CrossRef]
18. Gao, D.; Liu, Y.; Wang, T.; Wang, D. Experimental Investigation of the Impact of Coal Fines Migration on Coal Core Water Flooding. *Sustainability* **2018**, *10*, 4102. [CrossRef]
19. Zhang, J.; Han, S.; Zhang, C. Coal body structure identification by logging based on coal accumulation environment zoning and its application in Mabidong Block, Qinshui Basin. *Coal Geol. Explor.* **2021**, *49*, 114–122.
20. Zhuang, D.; Wang, Y.; Chen, Y. Study on Regularity of Coal Powder Production during CBM Well Drainage Based on Logging. *Coal Technol.* **2018**, *37*, 76–78.
21. Zhang, K.; Jiang, B.O.; Li, M. Identification and distribution of structure of seam No.3 in Xinjing Mine on the basis of well logs. *Coal Geol. Explor.* **2016**, *44*, 123–127+131.
22. Xiao, H.; Zhang, Z.; Guo, J. Coal structure identification method based on random forest combined with geophysical logging data and its application. *Sci. Technol. Eng.* **2021**, *21*, 10174–10180.
23. Wei, Y.; Meng, T.; Zhang, J. Relationship between coal reservoirs with different coal structures and the characteristics of coal fines produced in CBM well:a case study of Liulin block at the eastern margin of Ordos Basin. *Acta Pet. Sin.* **2023**, *44*, 1000–1014.
24. Zhang, Y.; Yang, Y.; Shao, G. Study on coal seam structure and properties of coal reserviors in Qinshui Basin. *Coal Sci. Technol.* **2017**, *45*, 131–136. [CrossRef]
25. Xian, B.; Liu, G.; Bi, Y.; Gao, D.; Wang, L.; Cao, Y.; Shi, B.; Zhang, Z.; Zhang, Z.; Tian, L.; et al. Coalbed methane recovery enhanced by screen pipe completion and jet flow washing of horizontal well double tubular strings. *J. Nat. Gas Sci. Eng.* **2022**, *99*, 104430. [CrossRef]
26. Wang, C.; Liu, Y.; Guo, G. Research on sweet spots of coalbed methane in Southern Shizhuang block of Qinshui Basin. *Clean Coal Technol.* **2016**, *22*, 102–107. [CrossRef]
27. Tan, X.; Ni, X.; Li, Z.; Xiong, Z.; Liu, X. An optimal selection method of wells for secondary fracturing in a single coal seam and its application. *Sci. Rep.* **2022**, *12*, 6098. [CrossRef] [PubMed]

28. Ni, X.; Zhao, Z.; Wang, Y.; Wang, L. Optimisation and application of well types for ground development of coalbed methane from no. 3 coal seam in shizhuang south block in Qinshui basin, Shanxi province, China. *J. Pet. Sci. Eng.* **2020**, *193*, 107453. [CrossRef]
29. Wei, Y.; Zhang, J.; Cao, D. Research status and thoughts for coal fines during CBM development. *Coal Geol. Explor.* **2020**, *48*, 116–124.
30. Tao, C.; Wang, Y.; Ni, X. Prediction model of coal–body structure and spatial distibution law based on logging parameters. *Coal Sci. Technol.* **2017**, *45*, 173–177+196.
31. Li, S.; Li, Z.; Wang, L. High rank coal structure and log interpretation method of fracture pressure in Shouyang block. *Coal Geol. Explor.* **2020**, *48*, 146–154.
32. Guo, C.; Xia, Y.; Wei, Z. Coalbed methane accumulation characteristics and type classification in Hancheng mining area. *J. China Coal Soc.* **2018**, *43*, 192–202.
33. Yao, Z.; Cao, D.; Wei, Y.; Li, X.; Wang, X.; Zhang, X. Experimental analysis on the effect of tectonically deformed coal types on fines generation characteristics. *J. Pet. Sci. Eng.* **2016**, *146*, 350–359. [CrossRef]